Heliyon 10 (2024) e39114

Contents lists available at ScienceDirect

Heliyon

journal homepage: www.cell.com/heliyon

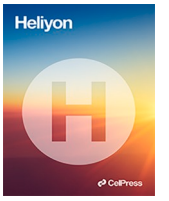

Research article

In-plane electrical conductivity of PEDOT:PSS/Halloysite composite thin films

Isidro Cruz-Cruz [a], Roberto I. Servín-Quintero [b], Luis Marcelo Lozano [b], Alan O. Sustaita [b,*]

[a] *Institute of Advanced Materials for Sustainable Manufacturing, Tecnologico de Monterrey, Av. Eugenio Garza Sada Sur 2501, Monterrey, 64849, Nuevo León, Mexico*

[b] *Tecnologico de Monterrey, School of Engineering and Sciences, Ave. Eugenio Garza Sada 2501, Monterrey, N.L., 64849, Mexico*

ARTICLE INFO

Keywords:
Conductive polymer
Composite films
Poly(3,4-ethylenedioxythiophene):poly(styrene sulfonate)
Halloysite nanotubes
Impedance spectroscopy
Secondary doping
Correlation length
Scaffold structure

ABSTRACT

PEDOT:PSS has found numerous applications in the field of advanced materials, especially in the development of organic electronics. Embedding nanoparticles into the polymer matrix has emerged as an effective strategy to modify the properties of PEDOT:PSS and develop advanced functional composites. Over the past decade, Halloysite nanotubes (HNT) have garnered significant interest and utility as nanofillers and/or templates due to their unique physical-chemical properties, small size, relatively low cost, and large availability. Interestingly, pairing PEDOT:PSS with non-conductive HNT has been demonstrated to enhance the charge transport properties of the composite film. Our discoveries show how the HNT can act as scaffolding for PEDOT:PSS by improving the local ordering of PEDOT chains and enabling the formation of conductive pathways. Consequently, the mechanism responsible for the observed changes in conductivity and the correlation between PEDOT:PSS and insulating nanofillers (HNT) could be different to that previously proposed. Hence, in this work it was observed that PEDOT:PSS/HNT composite films exhibited a non-linear conductivity dependence as a function of the HNT loading. From thermogravimetric analysis, infrared and UV-Vis-NIR spectroscopies, as well as impedance spectroscopy, a more complex interaction between the polymer chains and the nanotubes is revealed. Our study includes the modification of the interaction between the PEDOT chains and the nanofillers by using the secondary doping effect and functionalization of the nanotubes, which confirms our findings. These results represent a significant progress toward a deeper understanding of the emergence of a conductive polymer network on the nanofiller surface, leading to improvements in the electrical conductivity in the composite material.

1. Introduction

The development of technological products increasingly requires new materials and advanced processes, such as additive manufacturing, whilst keeping sustainability throughout the whole production line [1,2]. Regarding advanced materials, there is a growing interest in composites based on metals, ceramics, organic/polymer matrix phases, or a mixture of them, looking to satisfy the set of all possible requirements [2,3]. Particularly, in the field of flexible electronics, there is considerable attention on polymer

* Corresponding author.
E-mail address: alan.sustaita@tec.mx (A.O. Sustaita).

https://doi.org/10.1016/j.heliyon.2024.e39114
Received 19 September 2024; Accepted 8 October 2024
Available online 9 October 2024

composites with emerging developments in biomechanical engineering, harvesting energy, chemical or mechanical sensing, and lightweight-wearable devices, to name a few, due to their intrinsic biocompatibility and acceptable mechanical, chemical, and physical properties [1,4–9]. From all available alternatives, poly(3,4-ethylenedioxythiophene):poly(styrene sulfonate), or briefly PEDOT:PSS, stands out as a conjugated polymer that has attracted considerable attention since its first synthesis, due to its remarkable physicochemical characteristics [10]. To name some, it can be processed in aqueous dispersion at room temperature, and has remarkable film-forming properties, making it ideal for advanced manufacturing [11–13]. The PEDOT:PSS system combines the properties of two ionomers: PEDOT, a conjugated polymer that serves as a hole transport material, and PSS, which acts as a counterion to PEDOT, balancing the charge in the polymer system and promoting a stable dispersion of the conducting polymer in polar solvents, typically water. Despite the advantages granted by PSS, it is a non-conductive phase that tends to agglomerate forming insulating domains upon film formation, particularly on the surface. This, in turn, reduces the overall conductivity of the material. PSS is also hygroscopic and can contribute to the degradation of the films through the adsorption of environmental moisture. To address this issue, various strategies and extensive research have been developed to enhance the electrical characteristics and fine-tune the properties of PEDOT:PSS. This includes pre- or post-film formation treatments like careful control of the dispersion's pH [14], or the use of primary and/or secondary dopants [15–19]. In this manner, significant adjustments of both the electrical conductivity and the work function are obtained, ranging from 10^{-3} to 10^{3} S/cm, and from 4.0 to 5.0 eV, respectively [12,20–23]. Another strategy for customizing the properties of PEDOT:PSS is the incorporation of fillers into the polymer matrix, such as carbon nanostructures [9,24,25], metallic and metal oxide nanomaterials [26–28], and 2D materials [9,29]. Here, intending for potential applications on optoelectronics, halloysite nanotubes (HNT) are considered as nanofillers of a PEDOT:PSS polymer matrix.

Halloysite is a silico-aluminate clay with the structural formula of $Al_2Si_2O_5(OH)_4{\cdot}nH_2O$, sharing similarities in crystallographic structure and chemical composition with kaolinite. Halloysite nanotubes (HNT) are formed by rolled sheets of aluminosilicate, where the external face is predominantly composed of tetrahedral silica (SiO_2) and the inner face consists mainly of octahedral alumina (Al_2O_3) in a 1:1 stoichiometric ratio [30]. Each halloysite nanotube comprises 10–15 layers of aluminosilicate sheets, with a length ranging from 500 to 2000 nm and diameters falling within the range of 50–100 nm. The tube walls have an average thickness of 20 nm. It's worth noting that dimensions may vary significantly depending on the source of the deposit [31–34]. Potential applications for HNT stem from their weak hygroscopic nature, high porosity (with pore sizes in the 5–15 nm range and a moderate surface area of $<100\ m^2g^{-1}$ [35]); the charge difference in the faces of the tubes allowing for selective attachment of molecules to the walls [32]; and good cytocompatibility [36,37]. Furthermore, HNT are cost-effective and more readily available compared to other man-made nanofillers such as carbon nanotubes, being less than one-tenth of the cost and posing a lower environmental and biological risk [30,34]. Additionally, incorporating HNT into polymer materials has often resulted in multiple improvements to the properties of the composites, including enhanced thermal stability and flame retardancy [31,33]. Therefore, because HNT and PEDOT:PSS are biocompatible materials, they offer the opportunity to apply their composites in biomedical research, unlike the most commonly used carbon nanostructures [36,38].

To the best of our knowledge, studies on the potential applications of PEDOT:PSS/HNT composites have been limited. For instance, PEDOT/HNT composites were obtained through the chemical oxidative polymerization of PEDOT over HNT templates, exhibiting superior physicochemical properties compared to PEDOT. These properties include biocompatibility, corrosion resistance [39], electrochromic behavior [40], as well as enhanced electrical and thermal properties [41–43]. As for PEDOT:PSS/HNT composites, they have found applications in electromagnetic shielding devices [44], solar cells [45], and thermoelectric systems [46], owing to the improvements in the thermal and charge transport properties [47,48]. The enhancement in the conductivity has been explained as the result of a capillary effect, wherein the polymer chains of conductive PEDOT are compelled into well-ordered domains in the internal lumen surface, facilitating improved charge transport [48]. However, our findings indicate that the mechanism could be different due to the chemical characteristics of the two main components of the material, PEDOT and HNT.

This study investigates the impact of various HNT loadings on the optoelectronic properties of PEDOT:PSS/HNT composite films using FTIR and UV-Vis-NIR spectroscopies, along with Impedance Spectroscopy (IS) analysis. Surface morphology is evaluated through Scanning Electron Microscopy (SEM). Through these analyses, a significant change in the relative population of polarons/bipolarons in PEDOT:PSS was not observed in the presence of nanotubes in the composite films. Nevertheless, the improvement in the electrical properties of the material suggests a modification in the ordering of the delocalized domains of the conductive polymer chains. PEDOT:PSS/HNT composites were prepared in such a manner that only the interaction between these two materials is observed through in-plane electrical conductivity measurements. From the impedance characterization, the correlation length varied as a function of the HNT concentration, and the region where this phenomenon occurs is discussed. To complement our study, the use of dimethyl sulfoxide as a secondary dopant and the functionalization of HNT was also considered to modify the interaction between PEDOT:PSS and halloysite nanotubes. Understanding the charge transport mechanism opens the door for new potential applications for PEDOT:PSS/HNT composites in optoelectronics.

2. Experimental details

2.1. Sample preparation

Dow Corning glass slides served as substrates. Prior to their use, the slides underwent cleaning in an ultrasonic bath with acetone, followed by isopropanol and ethanol, each for 20 min. Subsequently, these were dried at 100 °C for 20 min and finally treated with UV light for 40 min.

Two PEDOT:PSS formulations were considered for this study: the first was provided by Sigma-Aldrich (conductive grade, 1.2 to 1.4

wt% solids content), and the second was supplied by Heraeus (Clevios^{TM} PT4). The latter formulation will be referred here as PT4.

PEDOT:PSS formulations were filtered using a 1 μm pore PES filter (Whatman® Puradisc), and the resulting amount of aqueous dispersion was used to calculate both the HNT concentration (by weight) and the isopropanol volume for the dispersion of the halloysite nanotubes. The ratio of weighted HNT to aqueous PEDOT:PSS was adjusted to achieve weight concentrations ranging from 0 to 0.5 % (for the formulation provided by Sigma-Aldrich) or from 0 to 5 % for PT4.

Halloysite nanotubes were acquired from Sigma Aldrich, with diameters and lengths within the range of 30–70 nm and 1–3 μm, respectively, as reported by the provider. The HNT were weighted and dispersed into isopropanol (iPrOH) using an ultrasonic bath operating at 40 kHz for 20 min. The iPrOH volume for the dispersion of the HNT was adjusted to achieve a PEDOT:PSS/iPrOH volume ratio of 2:1. For PT4, the 1:1 ratio (v/v) was also considered. Consequently, the HNT concentration in the alcoholic dispersion was not fixed; instead, the HNT and isopropanol contents were determined as a function of the PEDOT:PSS amount. Subsequently, PEDOT:PSS/HNT-iPrOH dispersions were prepared by mixing the filtered PEDOT:PSS with the alcoholic HNT dispersion in an ultrasonic bath for another 20 min. Following this, the PEDOT:PSS/HNT-iPrOH dispersions were spin-coated and then dried in an oven at 100 °C for 40 min in an air atmosphere. For discussion purposes, the aqueous PEDOT:PSS and the alcoholic PEDOT:PSS dispersions (prepared with similar iPrOH content but without HNT) were used and are referred to as PEDOT:PSS and 0 wt% HNT, respectively.

To complement the study, two additional sets of experiments were conducted: one considering secondary doping by the addition of dimethyl sulfoxide (DMSO) to the PEDOT:PSS/HNT dispersion, and the other involving the functionalization of halloysite nanotubes *via* octadecyltrichlorosilane (OTS). Composite thin films prepared with DMSO were prepared based on a previous work [16], where the optimal DMSO/PEDOT:PSS ratio was established as 1:5 by weight. The DMSO/PEDOT:PSS dispersion was prepared by magnetic stirring, after which it was mixed with the alcoholic dispersion of HNT using an ultrasonic bath, as previously described. The resulting thin films are labeled here as DMSO-PEDOT:PSS/HNT.

Functionalized halloysite nanotubes (*f*-HNT) were obtained by adapting the methods reported by C. Yegin et al. and A. B. Gurav et al., which were used for functionalizing SiO_2 nanoparticles [49,50]. In a typical process, 1.5 g of OTS (Sigma-Aldrich) was dispersed into 40 g of toluene (Sigma-Aldrich) in an ultrasonic bath for 3 min. Afterward, 2.1 g of HNT was added and mixed for an additional 3 min in the ultrasonic bath. The mixture was then left to rest in a covered flask at ambient temperature for 1 h. After this period, the excess toluene was decanted from the flask. Finally, the precipitated *f*-HNT were dried in an oven at 100 °C for 3 h to remove any remaining toluene [51]. PEDOT:PSS/*f*-HNT thin films were obtained through the same methodology described above for PEDOT:PSS/HNT composites.

2.2. Characterization and methods

Composite thin films on glass substrates were optically characterized using UV-Vis-NIR spectroscopy with a UV–Vis spectrometer (Cary, Agilent). As previously mentioned, the halloysite nanotubes were dispersed in isopropanol, and the resulting alcoholic dispersion was deposited on clean glass substrates. The UV–Vis spectra were collected after the isopropanol had evaporated.

FTIR measurements, with a resolution of 1 cm^{-1} in wavenumber, were obtained using a Frontier FTIR/FIR spectrometer (PerkinElmer) in transmission mode from spin-coated thin films over KBr pellets, which were dried in an oven for 40 min at 100 °C. The FTIR spectra of HNT and *f*-HNT were taken in the attenuated total reflectance (ATR) mode. These characterizations were performed at room conditions.

Thermogravimetric analysis (TGA) was performed to evaluate the thermal stability of the composites. Thermograms were recorded using a PerkinElmer thermogravimetric analyzer with a heating rate of 10 °C/min, from room temperature to 500 °C, under a N_2 atmosphere. For this, both PEDOT:PSS/HNT and PEDOT:PSS/*f*-HNT dispersions were drop-casted and dried in an oven at 100 °C for approximately 3 h to remove as much water as possible. Solid samples were then taken for analysis.

For electrical characterization, two parallel gold electrodes (1 mm wide, 1 cm long, and 20 nm thick) were sputtered (0.1 mbar, 2 nm/min Q150R ES, Quorum) onto the composite thin films using a custom-made shadow mask, defining a coplanar geometry with a 1 cm separation between the electrodes. Impedance spectroscopy (IS) measurements were obtained *via* a PalmSens 4 impedance analyzer with an AC sinusoidal signal of 30 mV in amplitude, in the frequency range of 10^{-1} to 10^{6} Hz. Other AC amplitudes were considered, but the best signal-to-noise ratio was observed under the mentioned conditions. All measurements were conducted inside a glove box filled with silica gel desiccant, maintaining a temperature around 25 °C and a relative humidity between 35 and 40 %.

Top-view microscopies and energy-dispersive X-ray spectroscopic (EDS) analyses were obtained *via* scanning electron microscopy (SEM, EVO MA25, ZEISS) for the spin-coated films, which were covered with a 5 nm gold layer through sputtering. Finally, the thickness of the electrodes and composite thin films was determined using a stylus profilometer (DextakXT, BRUKER) equipped with a 2-μm needle and a stylus force of 3 mg. For composite thin films, given their relatively high roughness, the thickness was calculated by integrating the profile area between two parallel scratches performed with a precision knife on the films and dividing it by the scanning length. This procedure was repeated twice in 3 different zones of the film for each sample, and the average value is reported as the nominal thickness.

3. Results and discussion

3.1. Interaction between PEDOT:PSS and halloysite nanotubes

Both PEDOT:PSS and HNT exhibit interesting physicochemical properties, as mentioned earlier. However, an initial challenge encountered with combining these materials was achieving a homogeneous mixture of the components. Due to the chemical

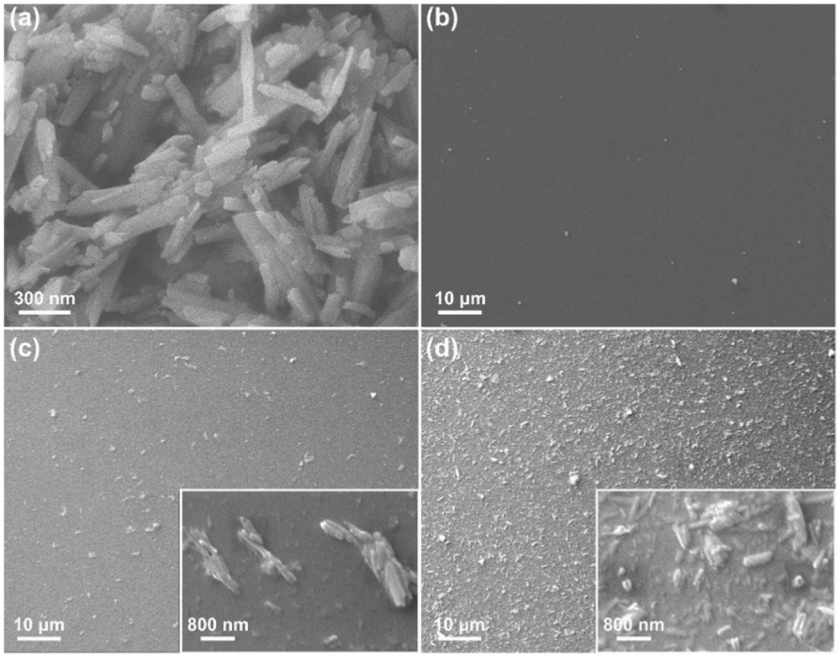

Fig. 1. SEM micrographs of (a) HNT after dispersing into isopropanol; and PEDOT:PSS/HNT composite thin films containing (b) 0, (c) 0.1, and (d) 0.5 wt% HNT. Agglomerates of HNT are also shown in the inset micrographs.

characteristics of HNT, the external surface is chemically inert and hydrophobic due to the Si – O – Si groups, while the internal lumen surface is hydrophilic in nature and chemically active owing to Al – OH functional groups [33]. In principle, this internal surface could facilitate the mixing of HNT into aqueous dispersion, however the pH of the dispersion media plays a crucial role [34]. In our initial attempts, without the assistance of isopropanol, the PEDOT:PSS/HNT dispersions were unstable, and the halloysite nanotubes precipitated shortly after completing the mixing process with PEDOT:PSS, for which the pH value was measured as 2.4 in our case. It has been reported that at this pH, HNT tend to form aggregates [34]. To address this, a premixing step was considered. HNT can be dispersed into polar solvents capable of hydrogen bonding [31,52]; therefore, methanol, ethanol, and isopropanol were tested. These solvents were chosen because they are compatible with PEDOT:PSS, although they tend to induce secondary doping [15,17]. Another potential approach for achieving stable HNT dispersions is adjusting the pH of PEDOT:PSS to higher values. However, this was not pursued here due to the unfavorable impact on the PEDOT:PSS properties [53]. The stability of the dispersion was assessed by considering the sedimentation time required for 10 mg of HNT in 5 ml of the solvent after mixing in an ultrasonic bath. Isopropanol resulted in good dispersion compared to the others, as HNT precipitated only after 30 min. In addition to the ultrasonic bath mixing, other alternatives like magnetic stirring and an ultrasonic tip (operating at 20 kHz) were also considered, but the ultrasonic bath proved to be the most effective method. It was observed that the mixing process could modify the length of the HNT. Measurements by DLS (nano25, Malvern, results not shown here) revealed that magnetic stirring does not alter the size distribution of the HNT ($d_{50} \sim 1$ μm, consistent with the supplier's specifications, D50), even after a processing time of 24 h. This observation has been reported previously [45]. On the other hand, both the ultrasonic tip and bath modified the HNT size distributions down to a few hundred nanometers ($d_{50} \sim 350$ nm, as seen in Fig. 1 a), but the size distribution promoted by the ultrasonic tip was broader than with the ultrasonic bath (standard deviations: ~218 nm and ~138 nm, respectively). After comparing the HNT before and after their dispersion in isopropanol, no modification in the optoelectronic structure was observed by UV–Vis and FT-IR spectroscopies, but only a change in the mean particle size was noted.

After the film forming, the surface quality of the PEDOT:PSS/HNT composite thin films was assessed by SEM. PEDOT:PSS thin films containing 0 wt% HNT (i. e., prepared from PEDOT:PSS + iPrOH dispersion only) exhibit a smooth surface with an average roughness of approximately 3 nm, as measured by profilometry. However, at the scale of tens of micrometers, the surface of composite films containing 0.1 wt% HNT increased its roughness up to ~10 nm, appearing relatively homogeneous (Fig. 1c), with only a few aggregates on the surface. HNT were dispersed randomly across the scanned area with random orientation. At high concentrations, there are regions where the nanotubes tend to aggregate; in some cases, they align parallel to each other, resembling a "bundle of sticks" (inset of Fig. 1c) while in other areas, they exhibit a disordered arrangement (inset in Fig. 1d). Additionally, the nanotubes are also oriented at a direction pointing out of the plane, contributing partially to the increased surface roughness of the films (~18 nm at 0.5 wt% HNT).

A thin PEDOT:PSS coating layer on the HNT is expected due to the strong electrical interaction arising from the negative charge on the external surface of the HNT and the positive charge on PEDOT segments. It occurs because the pH of the PEDOT:PSS aqueous dispersion is 2.4, and the HNT distribute their negative charge on their surface within a pH range of 2–9, as reported previously [54].

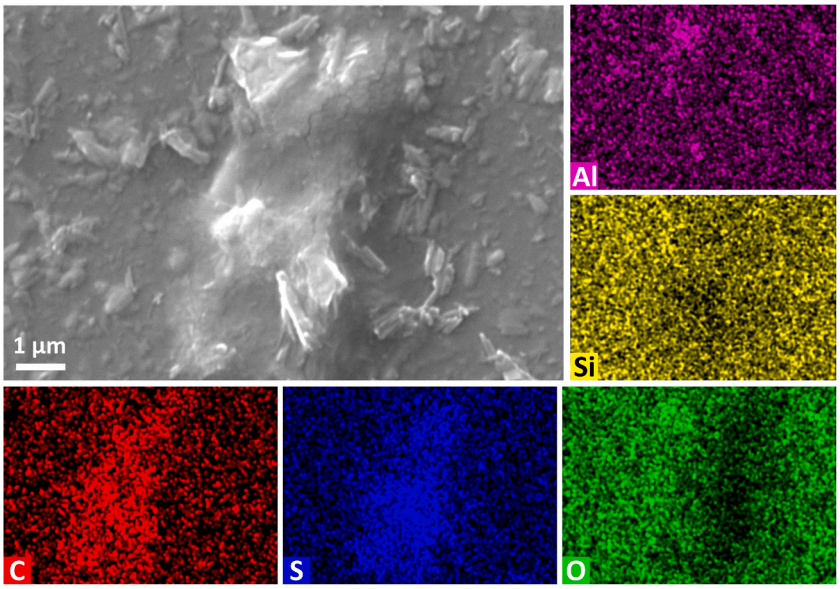

Fig. 2. Elemental mapping for spin-coated thin films (on glass substrate) based on PEDOT:PSS/HNT composites containing 0.5 wt% HNT. The signals from Al and Si in regions without HNT come from the substrate.

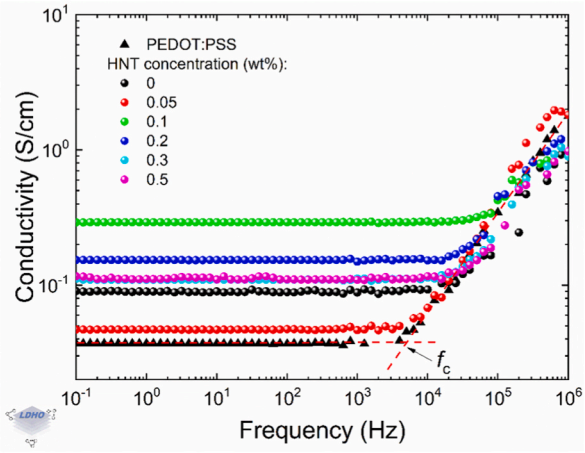

Fig. 3. Log – log plot of the conductivity modulus as a function of frequency for PEDOT:PSS/HNT composites. The critical frequency f_c was determined in the intermediate transition region by the intersection of straight lines, as indicated for pristine PEDOT:PSS thin films.

Additionally, upon adding iPrOH to PEDOT:PSS, no significant change in pH value was observed, indicating a similar electrostatic interaction between the materials. The presence of a thin PEDOT:PSS coating on the HNT aligns with findings in the literature, considering both oxidative polymerization and PEDOT:PSS formulations [41,45,48]. Elemental analysis revealed a uniform distribution of carbon and sulfur (belonging to both PEDOT and PSS chains) on the entire film, even over isolated HNT. However, the presence of these elements is highlighted on HNT agglomerates, as illustrated in Fig. 2.

To broaden the potential applications of PEDOT:PSS/HNT composites and gain new insights into their physical properties, the electrical characterization was conducted using impedance spectroscopy (IS). This technique is powerful as it allows the elucidation of various phenomena in a material or system based on the response to the applied alternating electromagnetic field. Charge carriers act as probes in the system under study, whereas they attempt to follow the input signal, thereby providing information about the time scales and/or distances at which the phenomena occur. While various methods, such as the colinear four-point probe, the var der Pauw method, or $I-V$ measurements with two electrodes in a sandwich configuration, can be used to characterize the electrical conductivity, IS measurements with electrodes in a coplanar configuration were selected here. This choice was influenced by the in-plane spatial distribution of the HNT in the composite thin films (mainly, but not exclusively) induced by the spin coating technique. Additionally, with this measurement configuration, a large number of halloysite nanotubes are evaluated, resulting in the observed response being the summation of all individual contributions. Studies conducted with out-of-plane measurements on PEDOT:PSS thin films containing

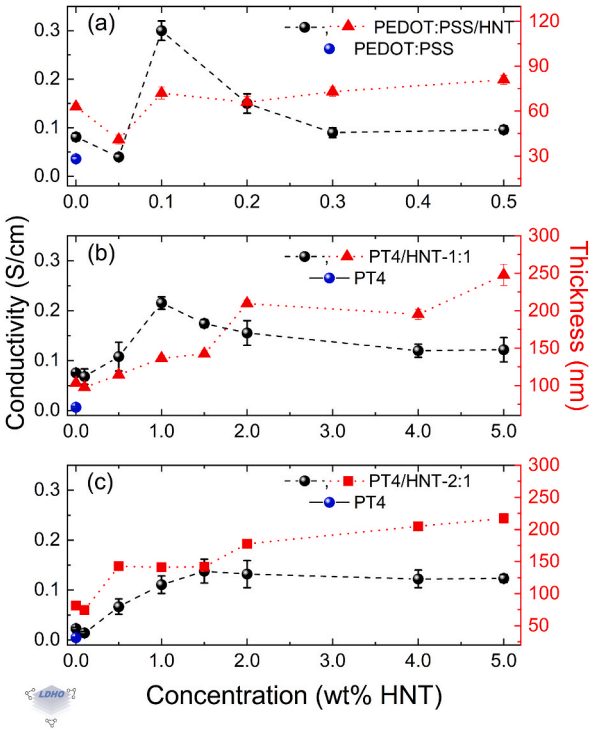

Fig. 4. Electrical conductivity (black symbols) and thicknesses (red symbols), as obtained at 100 Hz (DC regime) for PEDOT:PSS/HNT composites, as a function of the HNT concentration, for two PEDOT:PSS formulations. Sigma-Aldrich (a) and PT4 (b, c) at PEDOT:PSS to iPrOH volume ratios of 1:1 (b) and 2:1 (a, c). Blue symbols indicate the electrical conductivity for spin-coated thin films from the pristine PEDOT:PSS formulations. (For interpretation of the references to colour in this figure legend, the reader is referred to the Web version of this article.)

Table 1
Summary of results obtained from IS measurements for PEDOT:PSS/HNT composites.

HNT concentration (wt%)	Estimated critical frequency (kHz)	σ_{DC} (S/cm)	s
PEDOT:PSS	4.2	0.04 ± 0.01	0.71 ± 0.03
0	22.5	0.08 ± 0.01	0.64 ± 0.07
0.05	7.3	0.05 ± 0.01	0.76 ± 0.03
0.1	48.4	0.30 ± 0.02	0.64 ± 0.05
0.2	25.0	0.15 ± 0.02	0.62 ± 0.09
0.3	24.9	0.09 ± 0.01	0.67 ± 0.09
0.5	27.2	0.10 ± 0.01	0.64 ± 0.08

gold and silver nanoparticles can also be found in the literature [55].

As per previous reports, the DC electrical conductivity (σ_{DC}) tends to be enhanced by the addition of HNT to the matrix [42,45,48]. In these reports, solid samples in the form of pellets were considered for PEDOT/HNT composites obtained through the oxidative polymerization route [42], while PEDOT:PSS/HNT dispersions were deposited using casting or screen printing [45,48] rather than spin-coated thin films like in this study. No additives such as primary or secondary dopants (except iPrOH, as explained earlier) or plasticizers were considered for this first stage of our study. This deliberate choice aimed to avoid additional contributions to the observed behavior through additional factors like dipole-dipole or dipole-charge couplings. The discussion here only regards the interaction between PEDOT:PSS and HNT.

From the modulus of the total conductivity (σ) *vs* frequency (f) curves (Fig. 3), three distinct regions are observable: the DC regime at low frequencies (σ_{DC}, below 10^3 Hz) and the AC conductivity region at high frequencies where the electrical conductivity is linearly dependent on frequency (σ_{AC}, with a positive slope in the $log\ \sigma - log\ f$ plane), and an intermediate transition zone where the contributions of both the DC and AC components to the total conductivity become almost equally significant. The observed behavior in the $\sigma - f$ curves aligns with the characteristics typical of disordered solids, where the charge transport occurs through a hopping mechanism between localized sites in the material [56,57]. Considering the first region in the IS spectra, the σ_{DC} was obtained (Fig. 4a) and tabulated in Table 1. The electrical conductivity calculated from these measurements is similar to that obtained using the four-point probe technique [16], and particularly, the electrical conductivity of the pristine PEDOT:PSS film (0.04 ± 0.01 S/cm) matches the specifications provided by the supplier.

Table 2
Comparative data for several PEDOT:PSS/HNT composites.

[a] Conductivity for the composite materials (S/cm)	HNT loading	Enhancement (times)	Remarks	Ref.
Composites obtained by oxidative polymerization of EDOT				
1.66 {1 × 10^{-4}}	66.6 wt%	10^4	HCl as dopant. Composites in the form of Pellets.	[41]
9.35 {0.12}	40 wt%	77.9	Polymerization on PSS-grafted HNT. Composites in the form of Pellets.	[42]
12.89 {0.12}	50 wt%	107.4	Composites in the form of Pellets.	[43]
Composites obtained with commercial PEDOT:PSS formulations				
0.58 {0.17}	4 %	3.4	Drop casted films increase their conductivity up to 47.5 S/cm after treatment with FA.	[44]
381 {358}	1 wt%	1.1	The composite ink contains PH1000 formulation, 10 wt% EG, and 4 wt% polyurethane. Deposition by screen printing.	[45]
~0.55 {~0.15}	75.5 %	3.7	PH1000 formulation. Conductivity increases up to ~14 S/cm after treatment with 5 % PEG. Deposition by casting.	[48]
0.3 {0.04}	**0.1 wt%**	**7.5**	**Low conductive PEDOT:PSS formulation, deposited by spin coating.**	**This work**

HCl: hydrogen chloride, **FA**: formic acid, **EG**: ethyleneglycol and **PEG**: polyethylene glycol.
[a] The conductivity for the reference PEDOT used in each work is specified in curly brackets.

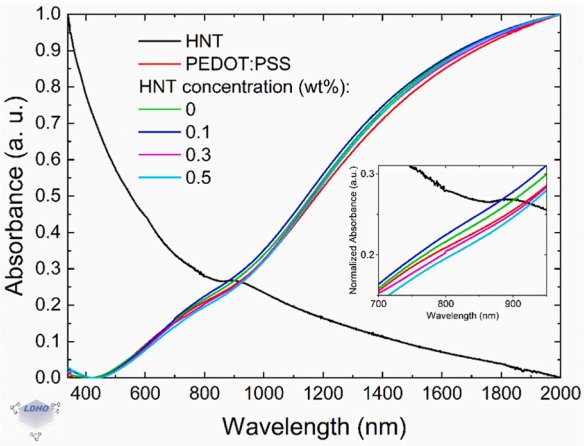

Fig. 5. Normalized UV-Vis-NIR spectra of PEDOT:PSS/HNT thin films. The inset shows the region around the polaronic band to highlight the effect of the HNT addition to PEDOT:PSS.

Spin-coated thin films prepared with PEDOT:PSS + iPrOH dispersion (0 wt% HNT) exhibited a slight increase in the conductivity by a factor of two compared to the pristine PEDOT:PSS films. This increase is attributed to the well-known secondary dopant effect [15, 17]. Certainly, this increase stands out slightlybecause the iPrOH content was not optimized here; it was just used to facilitate the mixing process of the halloysite with the aqueous PEDOT:PSS dispersion. Despite the secondary dopant effect induced by alcohol [17], the conductivity is influenced by the addition of insulating HNT into the films. Consequently, samples with 0.05 wt% HNT show a decrease in conductivity from 0.08 ± 0.01 to 0.05 ± 0.01 S/cm. Interestingly, an additional mechanism leads to a dramatic increase in the conductivity in the sample containing 0.1 wt% HNT. At this concentration, the films' conductivity increased by around eight times compared to the pristine PEDOT:PSS films, reaching 0.30 ± 0.02 S/cm. Further addition of HNT to the composites results in a reduction in electrical conductivity. The observed behavior in the σ_{DC} *vs* HNT concentrations plot is consistent with previous reports (see Table 2); however, the maximum value was achieved here with a lower loading of HNT.

The PT4 formulation was also considered to verify the observed behavior and possibly obtain new information. HNT concentrations for PT4-based composites varied from 0 to 5 wt% (Fig. 4b and c), reaching maximum conductivity values at 1.5 and 1 wt% HNT for the PT4/iPrOH volume ratios of 2:1 and 1:1, respectively. Despite the differences in the HNT concentrations resulting in the highest conductivity, the observed behavior was comparable for both PEDOT:PSS formulations. However, as the highest electrical conductivity was achieved with the PEDOT:PSS formulation provided by Sigma-Aldrich, only this formulation will be considered in the subsequent discussions. Note that the differences between the formulations concern the conductivity and the thicknesses of the thin films. The pristine PT4 thin film has an electrical conductivity of 0.01 S/cm, while the thicknesses of their composite films fall in the range of 60–250 nm.

Concerning the improvement in conductivity, it has been attributed to a capillary effect within the HNT whereby the PEDOT:PSS chains are dragged into the nanotubes [48]. However, because of the chemical nature of the four surfaces in halloysites exposed to the dispersion media – the internal hydrophilic lumen (chemically active), the external (chemically inert and hydrophobic), the interlayer

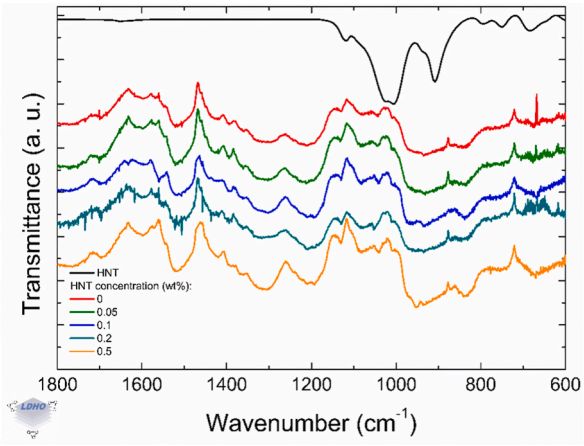

Fig. 6. FTIR spectra of PEDOT:PSS/HNT composite films at different HNT concentrations.

(chemically similar to the internal lumen surface), and the edge surfaces terminated by Al – OH and Si – OH groups [33] – the mechanism that promotes the enhancement in the charge transport could be different, at least in our case. The aluminol and siloxane groups in the edge surface might hinder the access of PEDOT molecules to the inner lumen surface. Consequently, optical characterizations were performed to elucidate possible modifications in the chemical or electronic structure of PEDOT:PSS that could account for the observed improvement resulting from the addition of relatively small amounts of HNT to PEDOT:PSS.

The normalized UV-Vis-NIR spectra of PEDOT:PSS/HNT thin films at different concentrations (Fig. 5) exhibit similar line shapes to the pristine PEDOT:PSS film, with their most intense absorbance bands in the near-infrared region. The use of normalized spectra is preferred here to emphasize differences associated with the relative population of bipolarons compared to polarons. This is achieved by comparing the relative intensity of absorbance bands located in the near-infrared region and between 700 and 900 nm, respectively, for each PEDOT:PSS/HNT composite film [19,58]. Despite the similarity in line shapes, there are slight differences that align with the observed electrical conductivity. Considering the normalized absorbance (inset of Fig. 5), at 800 nm it varies from 0.209 for the pristine PEDOT:PSS film to 0.216 for 0 wt% HNT. Subsequently, it increases to 0.224 at 0.1 wt% HNT, and then decreases to 0.205 at 0.3 wt% HNT, and finally drops to 0.196 at 0.5 wt% HNT. This could suggest a subtle difference in the relative charge carrier density. There seems to be a slight increase in the relative population of bipolarons as the HNT concentration increases because the band's intensity at 800 nm decreases. However, other possibilities should be considered, such as the energy storage of electromagnetic waves in small regions of the sample (near the halloysite nanotubes, for example), which may promote anomalous absorption akin to what is observed in thin metal-dielectric composites [59]. Additionally, differences in absorption capability may arise due to the rough surface of the materials. Pirouzfam and Sendur noted that the absorptance of randomly rough tungsten surfaces is sensitive to the correlation length and root-mean-square roughness of the surface in the visible and near-infrared regions [60]. However, a more detailed study on the absorption process in PEDOT:PSS/HNT thin films deposited by spin-coating is necessary.

FTIR spectra of pure HNT, and PEDOT:PSS films with various HNT concentrations are shown in Fig. 6 to get an insight into possible chemical modifications on the PEDOT backbone. Characteristic bands of PEDOT:PSS are observable at 1640, 1518 cm^{-1} (associated with C=C stretching in the PSS and PEDOT rings, respectively), 1340 cm^{-1} (C – C stretching in PEDOT's thiophene ring [61]), 1198 cm^{-1} (caused by the S=O stretching from PSS [61]), 1145 cm^{-1} and 1092 cm^{-1} (C – O stretching in PEDOT [61,62]) and finally, the bands at 936 cm^{-1}, 840 cm^{-1} and 691 cm^{-1} attributed to the C – S stretching of thiophene [61,62]. Any alteration in these bands or the emergence of new absorption bands following the addition of HNT would signify a change in the chemical environment of the PEDOT chains, resulting in a corresponding modification in the relative population of polarons and bipolarons. However, such a scenario is not observed here. Regarding to HNT, the characteristic bands corresponding to – OH vibrations in the inner lumen surface and the inner group (at 3696 cm^{-1} and 3624 cm^{-1}, respectively [63,64]), Si – O – Si (at 1028 cm^{-1}), the stretching of apical Si – O (at 684 cm^{-1} [64]) are clearly observable. Moreover, the band at 908 cm^{-1} is attributed to Al – O – OH vibrations [63], while the bands at 796 and 748 cm^{-1} could be attributed to O – H translation vibrations [65]. A very faint signal at 1644 cm^{-1} can be attributed to adsorbed water [63,64]. Comparing the spectra of pure HNT and PEDOT:PSS with the PEDOT:PSS/HNT composite films, no new bands were identified, and no noticeable shift or modification of the characteristic bands of the two main components was observed. This implies that any observable change in conductivity is not chemical in nature; instead, it is purely a physical phenomenon.

Using an excitation line of 514 nm, Raman spectroscopy was also considered to discern possible transitions between the aromatic and quinoid resonant structures in PEDOT due to the HNT addition (data not presented here). For this purpose, the laser spot was focused on various regions of the thin films, both with and without visible surface halloysite nanotubes, or their aggregates. The spectra collected from the surface of halloysite-rich regions (or their aggregates) exhibited the characteristic lineshape of PEDOT. However, after deconvoluting each spectrum into contributions coming from their quinoid and aromatic resonant structures [19], no significant differences were observed. It is worth noting that, due to the spot size of the 514 nm laser being ~1.5 μm, we were unable to confirm the PEDOT:PSS coating on HNT through Raman spectroscopy.

Returning to the analysis using IS, it is crucial to recall that in disordered materials the spatial and energetic distribution of localized

sites can be characterized by the correlation length (ξ). This parameter is associated with the averaged distance between localized regions in disordered solids [57]. As this parameter is dependent on the microstructure and the ratio of electrical conductivities of the phases within the solid, it provides valuable insights into the PEDOT:PSS/HNT composites. The Euclidian structure of the solid material is revealed when the charge carriers scan distances greater than the correlation length; otherwise, they exhibit high sensitivity to the fractal characteristics of the conducting network in the composite [66].

In a prior study, AC conductivity was utilized to elucidate how conductive grains are connected in PEDOT:PSS thin films as a result of secondary doping promoted by dimethyl sulfoxide [16]. In that research, AC measurements were also conducted in coplanar geometry, and the improvement in electrical conductivity was attributed to the reduction in the thickness of the PSS insulating barrier through phase segregation achieved with DMSO at the optimal loading. In contrast to that study, here, it is anticipated that the observed behavior is not a consequence of modifications in the PSS insulating barrier, at least over the whole material, as halloysites are neither acting as primary nor secondary dopants. In other words, HNT do not alter the PEDOT:PSS chemistry (as evidenced by unchanged FTIR bands) and they remain in the thin films. Regarding to secondary doping effect induced by isopropanol on the electrical properties of PEDOT:PSS/HNT composites, it does not account for the observed behavior in Fig. 3 because its content in the dispersion is nearly the same at different HNT concentrations, owing to the low amounts of HNT (less than or equal to 0.5 wt%). Thus, the observed behavior is exclusively a consequence of the presence of HNT in the films.

In classical percolation theory for composite systems with a conductive phase as filler, the DC conductivity above the percolation threshold follows the scaling law:

$$\sigma_{DC} = A \setminus (p - p_c)^t, \tag{1}$$

Where p is the mass fraction of the filler, p_c is the percolation concentration, A is the proportionality constant, and t is the conductivity exponent which depends on the system dimensionality and/or the correlation length ξ, depending on the authors or the model considered for its calculus [57,66]. From Fig. 4 and Tables 1 and it is evident that an interplay exists between two mechanisms governing the charge transport. The first mechanism dominates before the system reaches its maximum electrical conductivity at the optimal HNT concentration, while the second mechanism takes place afterward. The DC data in the initial region of Fig. 4 (up to the maximum conductivity value) can be fitted using Eq. (1). For instance, percolation concentrations for composites based on PT4-1:1 and PT4-2:1 dispersions are 0.56 % and 0.57 % by mass, with conductivity exponents of 0.46 and 0.86, respectively. The p_c values fall in the middle of the concentration range considered in this study. It is noteworthy that Eq. (1) applies to homogeneous systems with a conductive phase evenly distributed in an insulating matrix. However, in PEDOT:PSS/HNT composites, this is not the case because insulating HNT are discretely distributed in the conducting thin film at the micro scale. In other words, it is not a perfect mixture of insulating and conducting phases. This raises the question of where the percolation occurs.

At low frequencies, charge carriers travel a mean distance $L \propto f^{-1/2} > \xi$ in a Euclidian structure during a one-half period, overcoming a distribution of spatial randomly varying energy barriers. However, at frequencies higher than a critical one (f_c), they cover a mean distance $L \propto f^{-1/\delta} < \xi$, where δ can be associated with the fractal dimension of the conducting network or the level of bias imposed by the application of an external field [57,66]. At the limit between these two behaviors, charge carriers scan the distance that matches the correlation length at the critical frequency $f_c \propto \xi^{-\delta}$. PEDOT:PSS/HNT composite materials with relatively low DC conductivity exhibit a low critical frequency and, hence, a longer correlation length than materials with the highest DC conductivity, as evidenced in Table 1. The critical (or onset) frequency was estimated by calculating the intersection point between the fitted lines in the $log\ \sigma - log\ f$ plot, as shown in Fig. 3 [16,56]. Thus, in PEDOT:PSS/HNT systems the correlation length changes with the observed critical frequency, following the same trend as the DC conductivity. This suggests that the improvement in electrical conductivity in PEDOT:PSS/HNT composites can be linked to modifications in their correlation length as a function of the HNT concentration. However, it is crucial to consider another mechanism at concentrations higher than the optimal one. A clue about this mechanism is provided by the impedance spectra corresponding to the composite containing 0 wt% HNT. Its critical frequency is greater than that for pristine PEDOT:PSS, as noted in Fig. 3, which can be attributed to the secondary doping effect promoted by iPrOH and the consequent phase segregation, leading to a reduction in the PSS insulating barrier between conductive grains in the film. However, after the addition of 0.05 wt% HNT, the critical frequency decreases again, closely approaching the frequency value of the pristine PEDOT:PSS. Therefore, the addition of smaller amount of insulating phase increased the average correlation length of the thin film enough to promote a decrease in the conductivity. A similar effect at very low HNT content (0.1 wt%) in the composite films was also observed in PT4-based films (see Fig. 4b and c). The halloysite nanotubes could act as scattering centers at the lowest HNT concentration. At medium concentrations, their properties enhance charge transport in the films, and at concentrations higher than the optimal one, the charge scattering coupled with the amount of the insulating phase worsens the electrical conductivity.

The AC regime for disordered solids follows the approximated power law $\sigma(\omega) \propto \omega^s$, with $\omega = 2\pi f$ and $s \leq 1$, with the most common s values close to 0.8 [67]. The s exponents for PEDOT:PSS/HNT composites (Table 1) are in the range of 0.62–0.76, slightly below 0.8, confirming that the transport mechanism is due to hopping.

To verify the universality of the conductivity *vs* frequency behavior, master curves can be constructed by scaling the conductivity values to the DC conductivity and the frequency through a scaling factor $A_{\xi,c}$ that depends on the f_c and the critical reference frequency $f_{c,ref}$, or directly on the correlation length ξ [66,68]. The master curves in Fig. 7 were constructed by taking as a reference curve one belonging to the pristine PEDOT:PSS film. Thus, each f_c value was divided by $A_{\xi,c} = f_c/f_{c,ref}$ because the reference curve has the lowest DC conductivity. It is worth mentioning that Laibowitz and Gefen experimentally determined that the scaling factor can also be expressed as a function of $\xi^{2+\theta}$ [68], where $2+\theta$ is related to the fractal dimension of the material. From Fig. 7, the experimental data appears to be in rough agreement with the approximate power-law model, and it applies to the entire set of HNT concentrations

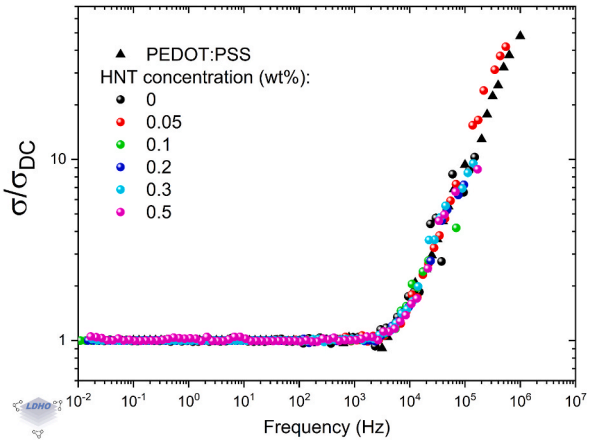

Fig. 7. Master curve showing scaled conductivity vs scaled frequency.

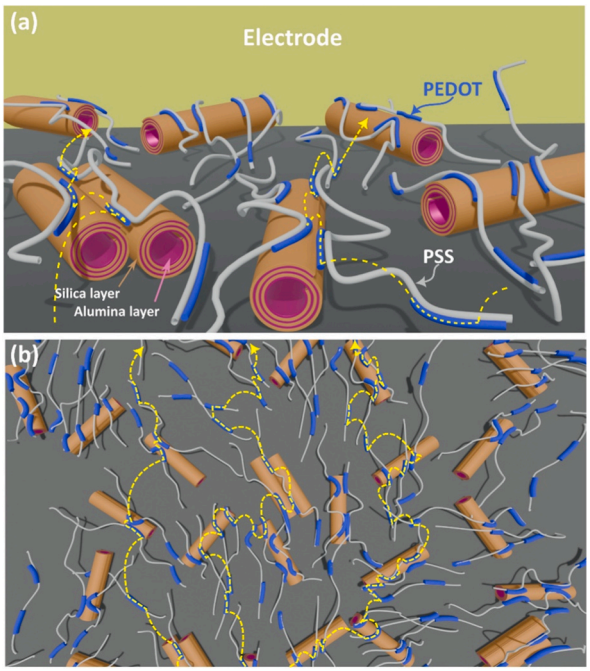

Fig. 8. Proposed mechanism for charge transport in PEDOT:PSS/HNT composites. Two possible trajectories for charge carriers are shown with dashed yellow lines in (a), demonstrating the reduction in correlation length facilitated by the HNT. In (b), charge carrier scattering promoted at relatively high HNT concentrations is schematically depicted. (For interpretation of the references to colour in this figure legend, the reader is referred to the Web version of this article.)

considered here. In other words, the observed behavior for a given conductivity and HNT concentration is equivalent to that for the reference conductivity curve.

Due to the observed behavior, localized regions of well-ordered domains of PEDOT:PSS are formed because of the addition of halloysites, which modifies the effective correlation length. Referring to Fig. 1, potential regions for the formation of conductive pathways in the PEDOT:PSS/HNT thin films are: **1)** the space between HNT aggregates containing PEDOT:PSS only, **2)** the internal lumen surface of halloysites, **3)** nanotube boundaries when halloysite bundles are formed, and **4)** the surface of the nanotubes.

The interlayer space (approximately 0.7 nm [37]) and the edge surfaces terminated are disregarded due to the size of PEDOT:PSS particles (a few tens of nm) and because of the hindering effect promoted by the edge surfaces terminated by aluminol and siloxane groups. Considering the first option, the spaces in between the HNT aggregates do not explain the observed behavior in the conductivity due to the absence of halloysites, thus, it is also possible to discard this possibility.

Regarding the second alternative, in a previous study, the enhancement in conductivity was achieved at a much higher HNT concentration than in this study. In that work, the improvement was attributed to the formation of conductive pathways within the

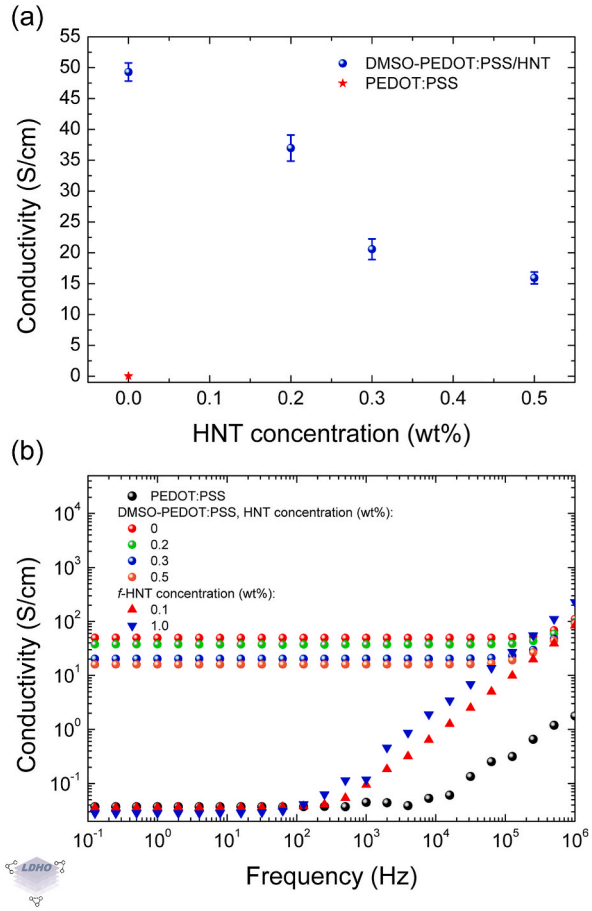

Fig. 9. Electrical conductivity of DMSO-PEDOT:PSS/HNT thin films as a function of the HNT concentration: DC regime (a), and conductivity as a function of frequency (b). In (b), the AC conductivity for PEDOT:PSS/*f*-HNT thin films is also shown.

halloysite nanochannels due to the strong capillary effect, facilitated by its highly hydrophilic nature, which fills the lumen of HNT with PEDOT:PSS [48]. However, the mechanism here appears to be different, likely due to the lower conducting PEDOT:PSS formulations used, compared to Clevios PH1000. The loading capacity of halloysite nanochannels depends on various factors including the morphology of the nanotubes, pH, the solvent (water + isopropanol in our case) [34], and, of course, the molecular nature of the lumen filler. Previous reports, related to the chemical polymerization of PEDOT [62], support that the conducting channel in the lumen is less feasible. According to the work by F. Wang et al. on the PEDOT synthesis with PSS grafted onto HNT template [42], chemical polymerization occurred in both the lumen and the HNT external surface, but it was preferably on the latter one due to the negatively grafted PSS. It was also observed during the chemical oxidation polymerization of EDOT with HNT [43], where PEDOT was mainly deposited on the outside surface of HNT due to the positively charged PEDOT balancing the negatively charged outer surface of HNT. However, PEDOT polymerization can also take place in the interlayers of HNT under specific synthesis conditions [41]. The polymerization on the outer surface of HNT is favored by the presence of surface defects and additionally, the PEDOT coating also depends on the proportion EDOT to HNT [40]. For instance, at a relatively low EDOT to HNT proportion (1:3) the polymerization occurred on the surface of HNT rather than in the precursor solution, resulting in a PEDOT thickness of about 8 nm, with the lumen clearly visible by TEM. In this manner, the formation of conductive pathways in the internal lumen surface is also unlikely.

If even the EDOT monomer preferably polymerizes on the halloysite surface, then PEDOT will favorably deposit on this surface due to its positive charge at low pH. This means that the third and fourth alternatives mentioned earlier are possible. Note that these two options are similar due to the strong interaction between the HNT and PEDOT chains at low pH, as polymer chains are closely packed and promote the formation of conductive pathways on the nanotube surface, or even in between the nanotube bundles, which modify the average correlation length in the composite, as depicted in Fig. 8. The importance of the interaction between charged species and HNT has been evidenced in previous reports. For example, negatively charged insulin, a high molecular weight substance, was released at a rate of ~70 % within 140 h in water. However, the release process was accelerated by 50 times in the presence of a positively charged polyelectrolyte [69]. Additionally, it was observed that the interaction of a cationic polymer occurs with the negative surface of the nanotube at low pH, whereas anionic ones interact with the positively charged inner surface, and no specificity was observed with nonionic polymers [70].

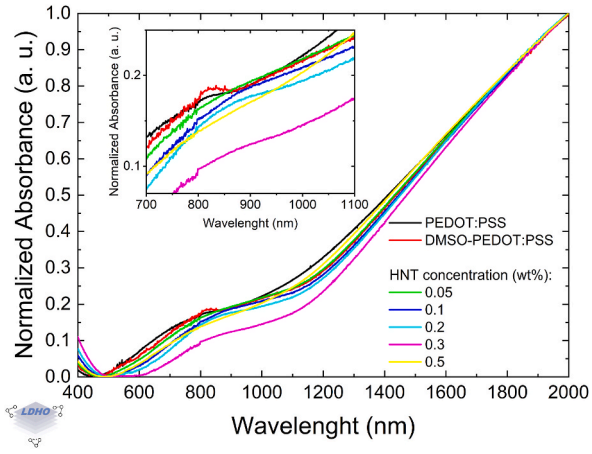

Fig. 10. Normalized UV–Vis spectra for DMSO-PEDOT:PSS/HNT thin films, containing a DMSO/PEDOT:PSS ratio of 1:5 by weight. The peak at around 800 nm for the PEDOT:PSS/DMSO film (the red curve, clearly visible in the inset) is an artifact introduced during the measurement process. (For interpretation of the references to colour in this figure legend, the reader is referred to the Web version of this article.)

Based on our experimental evidence, it is possible to elucidate a conceivable mechanism for the enhancement in conductivity at low HNT contents. As mentioned earlier, at low pH, the lumen of halloysite possesses an increased positive charge, while negative charges remain on the surface. These charges influence the aggregation and dispersion of halloysites in aqueous media, as well as their interactions with charged molecules [34]. Upon applying an external electric field, the charge carriers cover the distance between the electrodes *via* a hopping mechanism between localized regions. Changes in the correlation length due to the strong electrical interaction between the PEDOT chains and halloysite nanotubes are observed by impedance spectroscopy. According to this characterization technique, the correlation length diminishes, and consequently the critical frequency, roughness, phase segregation and conductivity increase (Fig. 8a). However, at higher HNT concentrations than the optimal one, a second mechanism becomes important, related to the increased amount of the insulating phase and charge carrier scattering that hinder the effective charge transport (Fig. 8b).

3.2. *Modification of the interaction between PEDOT:PSS and halloysite nanotubes*

The electrical properties of PEDOT:PSS/HNT composites can be tailored using strategies previously reported in the literature. Thus, in the second stage of our study, additional experiments were conducted considering secondary doping by the addition of dimethyl sulfoxide (DMSO) to the PEDOT:PSS/HNT dispersion, as well as the functionalization of halloysite nanotubes *via* octadecyltrichlorosilane (OTS). The conductivity as a function of frequency for both conditions is shown in Fig. 9.

DMSO is a well-known compound that promotes phase segregation in PEDOT:PSS thin films due to its high dipole moment (4.3 D). Based on previous work [16], the optimal DMSO/PEDOT:PSS ratio was established as 1:5 by weight for enhancing the electrical conductivity; therefore, the same DMSO concentration was used in this study. An improvement in the charge transport in the film regions between the HNT is expected, whereas the interaction between the PEDOT chains and HNT is probably weakened.

The secondary doping effect promoted by DMSO addition is verified by the enhancement in the conductivity in more than three orders of magnitude (from 0.04 to 49.25 S/cm), as shown in Fig. 9a. This is indicative that the correlation length in PEDOT:PSS/DMSO films (0 wt% HNT) decreased in comparison to that in the pristine PEDOT:PSS material, through phase segregation, as previously reported [16]. Afterward, when the HNT concentration increases, the insulating nature of the HNT becomes important in such a way that randomly distributed HNT hinder the charge transport. As a result, the conductivity monotonically decreases as a function of the HNT concentration (Fig. 9a).

The addition of DMSO reduces the correlation length of the material compared to pristine PEDOT:PSS thin films, as indicated by the shift of the critical frequency towards values close to the instrument's measurement range (see Fig. 9b). With the addition of HNT (from 0 to 1 wt%), the critical frequency f_c is slightly modified as a function of the HNT concentration, ranging from 1.6×10^5 to 3.5×10^5 Hz. Thus, the effect promoted by the interaction between HNT and PEDOT chains is overshadowed by the secondary doping effect. This observation justifies our initial interest in studying PEDOT:PSS/HNT systems without any other additives.

Moreover, UV–Vis spectroscopy (Fig. 10) confirmed that the relative population of polarons or bipolarons does not change in PEDOT:PSS/DMSO films as compared to pristine PEDOT:PSS material (both have the same line shape and relative band intensities). This indicates that the enhancement in the electrical conductivity can be attributed to a change in the correlation length promoted by phase segregation [16]. The enhanced conductivity in PEDOT:PSS/DMSO films (at 0 wt% HNT) decreases monotonically as a function of the HNT loading, while the polaronic band at around 800 nm slightly diminishes. This suggests that the relative population of bipolarons in composites containing HNT is slightly greater than in pristine PEDOT:PSS thin films, indicating that the interaction between the PEDOT chains and HNT still exists.

The decrease in conductivity of PEDOT:PSS/HNT systems as a function of HNT concentration when additives are used has been

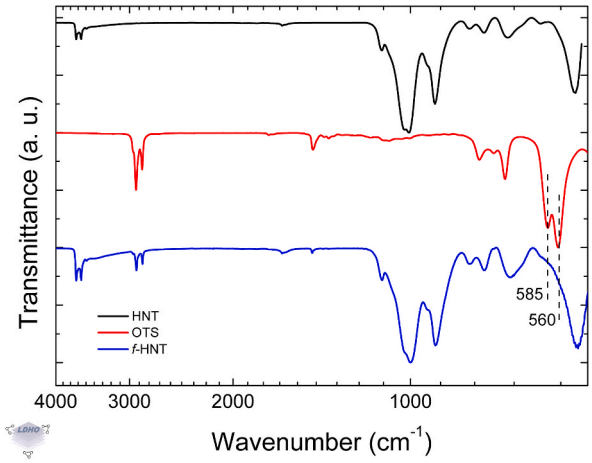

Fig. 11. Semi-log plot showing the FTIR spectra for HNT, OTS and *f*-HNT.

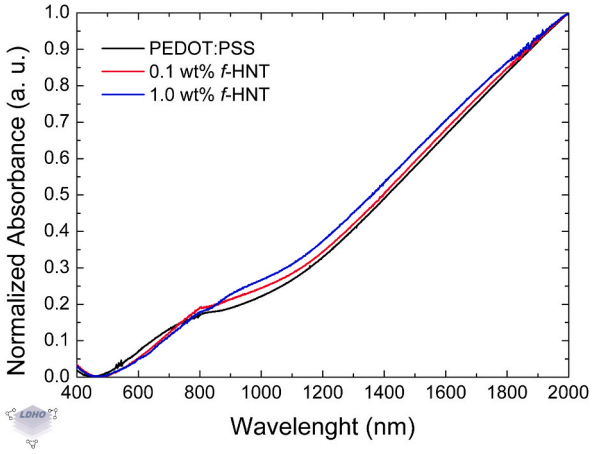

Fig. 12. UV–Vis spectra for PEDOT:PSS/*f*-HNT thin films.

previously observed by H. Yan et al., with formic acid and ethylene glycol [48], S. Tu et al. with DMSO/salts [46] and by P. Gemeiner et al., using ethylene glycol [45]. In DMSO-PEDOT:PSS/HNT systems, phase segregation is the most critical factor contributing to improved charge transport rather than the interaction between HNT and PEDOT chains at relatively low HNT contents. HNT hinder charge transport.

The functionalization of the HNT (*f*-HNT) was conducted using the procedure described in the experimental section. This procedure is applicable to HNTs because their external surface is composed of Si—O—Si functional groups.

In the FTIR spectra of the PEDOT:PSS/*f*-HNT composites (Fig. 11), the absence of the characteristic double band at 650 cm^{-1} and 585 cm^{-1}, assigned to the Si – Cl stretching of OTS, confirms the functionalization of HNT [49]. Due to the functionalization process, the interaction between the external HNT surface and PEDOT:PSS is hindered, leading to expected changes in electrical conductivity and correlation length. As shown in Fig. 9b, the DC conductivities for PEDOT:PSS/*f*-HNT composites at two different concentrations (0.1 and 1.0 wt%) are of the order of pristine PEDOT:PSS films but with a higher correlation length (the critical frequency decreased). This indicates that the interfacial functional groups hinder the interaction between the PEDOT chains and the external surface of the halloysites, and the insulating phase in the composite only impedes charge transport.

PEDOT:PSS/*f*-HNT thin films showed larger aggregates than composite films without functionalized HNT, resulting in more significant uncertainty in the films's thicknesses (a useful parameter for conductivity calculation), which may lead to a probable overestimation of the electrical conductivity. This explains the subtle differences between the calculated conductivities of films with *f*-HNT and pristine PEDOT:PSS. However, the correlation length clearly increased as a function of the *f*-HNT content, as seen in Fig. 9.

Considering the UV–Vis spectra of PEDOT:PSS/*f*-HNT thin films (Fig. 12), the difference between them is subtle, with the relative intensity of the polaronic band almost unaltered. Thus, functionalized halloysite nanotubes do not modify the relative population of bipolarons in PEDOT. Therefore, due to the weakened interaction between HNT and PEDOT chains, there is no significant contribution to the improvement in charge transport, in fact, it may even be hindered.

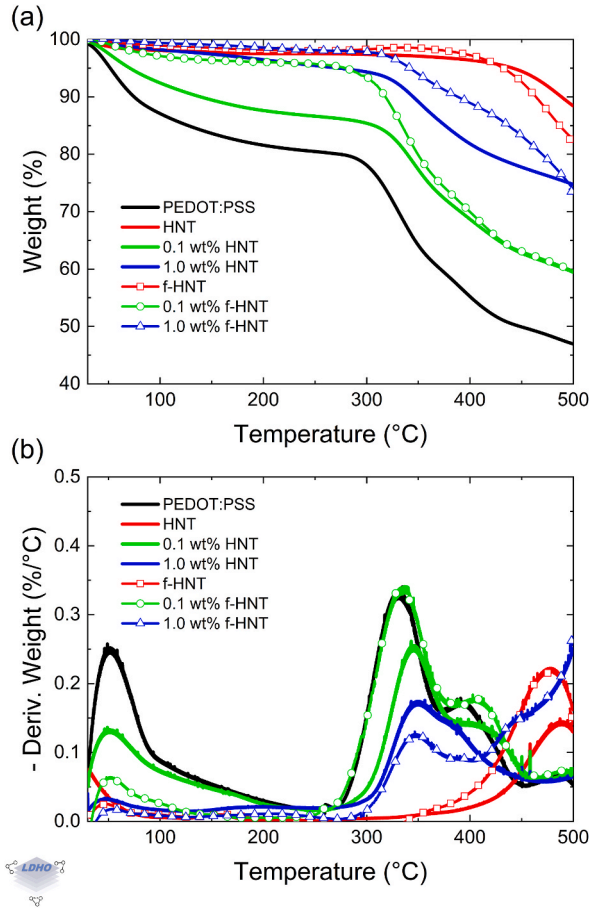

Fig. 13. TG and DTG curves of PEDOT:PSS/HNT composites.

Thermogravimetric analysis was performed to evaluate the role of both HNT and *f*-HNT in the thermal stability of the composites, as depicted in Fig. 13. The thermal properties of HNT are not affected by their dispersion in isopropanol in an ultrasonic bath [45]. The thermal stability of PEDOT:PSS/HNT composites improved as a function of the nanofiller content compared to the pristine PEDOT:PSS thin films. Similar behavior has been observed previously [41,71–74].

Regarding the nature of the degradation processes, the derivative thermogram (DTG) curves (Fig. 13b) exhibit the first peak associated with residual water loss in the materials. The second peak between 300 °C and 350 °C has been attributed to the decomposition temperature of PSS (due to the removal of polystyrene sulfonate groups), and the third, at temperatures higher than 390 °C, to degradation of the polymer backbone and decomposition of the aromatic thiophene ring of PEDOT [41,75–77]. However, different assignments for these thermal processes can be found in the literature, depending on the polymer chain lengths or the PEDOT content in the composite [78–80]. In the case of halloysites, the peak at temperatures higher than 450 °C is related to structural water loss [41].

The presence of HNT (or *f*-HNT) in the composites restricts the thermal motion of the polymer chains, PEDOT and PSS, delaying the degradation process of the polymers, as seen in Fig. 13a. Halloysite nanotubes degrades at 450 °C (onset) and, after functionalization, at 420 °C (onset). The composites follow the same trend. For instance, after water removal, the thermal degradation onset for composites containing 0.1 wt% HNT changes from 320 °C to 300 °C when the nanotubes are functionalized. However, considering thermal processes below 300 °C, the percentage of mass loss for composites containing HNT is greater than for *f*-HNT-based materials, suggesting a modification in the interaction between PEDOT, PSS and HNT. From the electrical characterization, the interaction between PEDOT chains and HNT is weakened after the functionalization process.

4. Conclusions

PEDOT:PSS/HNT composites were spin-coated onto glass substrates and their optoelectronic properties were studied. The results presented earlier offer new insights into the interaction between PEDOT:PSS and HNT, enabling various potential applications. An increase in conductivity was observed after adding halloysites nanotubes to the PEDOT:PSS conducting matrix. Although the electrical conductivity is not as high as that obtained with secondary dopants, the condition of relatively low conductivity is not a restriction but

an opportunity for using PEDOT:PSS/HNT thin films in optoelectronic devices which do not require a high-conductivity state, while taking advantage of the hollow structure of the HNT.

The PEDOT:PSS formulations considered here exhibited similar behavior to that previously reported in the literature; however, in our case, the maximum electrical conductivities were achieved at lower HNT concentrations. This difference could be attributed to variations in the specific properties of the PEDOT:PSS formulations used, such as particle size, viscosity, or solid content, as well as the thin film-forming process considered here (spin-coating).

Based on the different characterization techniques conducted on the composite thin films, the conductivity enhancement is attributed to the formation of conductive pathways on the HNT surface, which makes hopping transport more efficient. UV–Vis spectroscopy did not reveal significant modifications in the relative population of polarons and bipolarons, nor were there observed chemical changes. However, the observed small variations in the absorbance at ~800 nm could suggest a strong electrical interaction between HNT and PEDOT chains at low pH values. Moreover, our findings from impedance spectroscopy support the notion that the correlation length in the PEDOT:PSS/HNT composites decreases. Finally, the optoelectronic properties of composite materials modified *via* the secondary doping effect and functionalization of the halloysite nanotubes are consistent with the proposed mechanism.

The addition of HNT increases the surface roughness of films. This factor must be considered during the design of opto-electronic devices. Special procedures need to be developed to ensure proper distribution of HNT and better stability of dispersions.

CRediT authorship contribution statement

Isidro Cruz-Cruz: Formal analysis, Investigation, Methodology, Validation, Writing – review & editing, Conceptualization, Data curation. **Roberto I. Servín-Quintero:** Conceptualization, Data curation, Investigation, Methodology, Writing – original draft. **Luis Marcelo Lozano:** Funding acquisition, Writing – review & editing, Visualization. **Alan O. Sustaita:** Formal analysis, Investigation, Project administration, Resources, Supervision, Writing – review & editing, Conceptualization, Validation, Writing – original draft.

Data availability

Data used for this work is available upon request to the corresponding author.

Declaration of competing interest

The authors declare that they have no known competing financial interests or personal relationships that could have appeared to influence the work reported in this paper.

Acknowledgments

The authors thank Tecnologico de Monterrey for providing financial resources for materials and covering tuition fees. We express our gratitude to CONAHCYT (Consejo Nacional de Humanidades, Ciencia y Tecnología de México) for the support to this work through the maintenance scholarship No. 818081 for graduate studies. This work was supported by the Laboratory of Optoelectronic Hybrid Devices (LDHO). The authors are thankful to the Manufacturing Laboratory of the Center for Innovation in Digital Technologies. The authors would also like to thank PhD. Valery Moreno-Vega, M.Sc. Martín Francisco Jiménez-Moreno (CIDiTec), and M.Sc. Mauricio Binny Jind-Aguirre for providing their help with conductivity analysis, and M.Sc. Regina Vargas-Mejía (CIDiTec) for her great assistance in getting SEM images.

References

[1] Y. Huang, S. Kormakov, X. He, X. Gao, X. Zheng, Y. Liu, J. Sun, D. Wu, Conductive polymer composites from renewable resources: an overview of preparation, properties, and applications, Polymers 11 (2019) 187, https://doi.org/10.3390/polym11020187.

[2] S. Ford, M. Despeisse, Additive manufacturing and sustainability: an exploratory study of the advantages and challenges, J. Clean. Prod. 137 (2016) 1573–1587, https://doi.org/10.1016/j.jclepro.2016.04.150.

[3] N. Guo, M.C. Leu, Additive manufacturing: technology, applications and research needs, Front. Mech. Eng. 8 (2013) 215–243, https://doi.org/10.1007/s11465-013-0248-8.

[4] S.M.A. Mokhtar, E. Alvarez De Eulate, M. Yamada, T.W. Prow, D.R. Evans, Conducting polymers in wearable devices, Med. DEVICES Sens. 4 (2021) e10160, https://doi.org/10.1002/mds3.10160.

[5] B. Sun, G. Zhou, T. Guo, Y.N. Zhou, Y.A. Wu, Biomemristors as the next generation bioelectronics, Nano Energy 75 (2020) 104938, https://doi.org/10.1016/J.NANOEN.2020.104938.

[6] G. Kaur, R. Adhikari, P. Cass, M. Bown, P. Gunatillake, Electrically conductive polymers and composites for biomedical applications, RSC Adv. 5 (2015) 37553–37567, https://doi.org/10.1039/C5RA01851J.

[7] J. Chen, Y. Zhu, J. Huang, J. Zhang, D. Pan, J. Zhou, J.E. Ryu, A. Umar, Z. Guo, Advances in responsively conductive polymer composites and sensing applications, Polym. Rev. 61 (2021) 157–193, https://doi.org/10.1080/15583724.2020.1734818.

[8] G. Prunet, F. Pawula, G. Fleury, E. Cloutet, A.J. Robinson, G. Hadziioannou, A. Pakdel, A review on conductive polymers and their hybrids for flexible and wearable thermoelectric applications, Mater. Today Phys. 18 (2021) 100402, https://doi.org/10.1016/j.mtphys.2021.100402.

[9] C. Gao, G. Chen, Conducting polymer/carbon particle thermoelectric composites: emerging green energy materials, Compos. Sci. Technol. 124 (2016) 52–70, https://doi.org/10.1016/j.compscitech.2016.01.014.

[10] A. Elschner, S. Kirchmeyer, W. Lovenich, U. Merker, K. Reuter, PEDOT: Principles and Applications of an Intrinsically Conductive Polymer, 0 ed., CRC Press, 2010 https://doi.org/10.1201/b10318.

[11] K. Sun, S. Zhang, P. Li, Y. Xia, X. Zhang, D. Du, F.H. Isikgor, J. Ouyang, Review on application of PEDOTs and PEDOT:PSS in energy conversion and storage devices, J. Mater. Sci. Mater. Electron. 26 (2015) 4438–4462, https://doi.org/10.1007/s10854-015-2895-5.

[12] G. Huseynova, Y. Hyun Kim, J.H. Lee, J. Lee, Rising advancements in the application of PEDOT:PSS as a prosperous transparent and flexible electrode material for solution-processed organic electronics, J. Inf. Disp. 21 (2020) 71–96, https://doi.org/10.1080/15980316.2019.1707311.

[13] M. Criado-Gonzalez, A. Dominguez-Alfaro, N. Lopez-Larrea, N. Alegret, D. Mecerreyes, Additive manufacturing of conducting polymers: recent advances, challenges, and opportunities, ACS Appl. Polym. Mater. 3 (2021) 2865–2883, https://doi.org/10.1021/acsapm.1c00252.

[14] F.-F. Pang, S. Li, W.-Q. Sun, G.-Z. Han, Reversible conductivity modulation of PEDOT:PSS based on pH, Mater. Chem. Phys. 186 (2017) 246–250, https://doi.org/10.1016/j.matchemphys.2016.10.050.

[15] J. Ouyang, "Secondary doping" methods to significantly enhance the conductivity of PEDOT:PSS for its application as transparent electrode of optoelectronic devices, Displays 34 (2013) 423–436, https://doi.org/10.1016/j.displa.2013.08.007.

[16] I. Cruz-Cruz, M. Reyes-Reyes, M.A. Aguilar-Frutis, A.G. Rodriguez, R. López-Sandoval, Study of the effect of DMSO concentration on the thickness of the PSS insulating barrier in PEDOT:PSS thin films, Synth. Met. 160 (2010) 1501–1506, https://doi.org/10.1016/j.synthmet.2010.05.010.

[17] X.S. Rozhkova, A.K. Aimukhanov, B.R. Ilyassov, A.K. Zeinidenov, The role of alcoholic solvents in PEDOT:PSS modification as hole transport layers for polymer solar cells, Opt. Mater. 131 (2022), https://doi.org/10.1016/j.optmat.2022.112708.

[18] T.C. Wei, S.H. Chen, C.Y. Chen, Highly conductive PEDOT:PSS film made with ethylene-glycol addition and heated-stir treatment for enhanced photovoltaic performances, Mater. Chem. Front. 4 (2020) 3302–3309, https://doi.org/10.1039/d0qm00529k.

[19] M. Reyes-Reyes, I. Cruz-Cruz, R. López-Sandoval, Enhancement of the electrical conductivity in PEDOT: PSS films by the addition of dimethyl sulfate, J. Phys. Chem. C 114 (2010) 20220–20224, https://doi.org/10.1021/jp107386x.

[20] D. Alemu, H.Y. Wei, K.C. Ho, C.W. Chu, Highly conductive PEDOT:PSS electrode by simple film treatment with methanol for ITO-free polymer solar cells, Energy Environ. Sci. 5 (2012) 9662–9671, https://doi.org/10.1039/c2ee22595f.

[21] I. Cruz-Cruz, M. Reyes-Reyes, R. López-Sandoval, Formation of polystyrene sulfonic acid surface structures on poly(3,4-ethylenedioxythiophene): poly (styrenesulfonate) thin films and the enhancement of its conductivity by using sulfuric acid, Thin Solid Films 531 (2013) 385–390, https://doi.org/10.1016/j.tsf.2012.12.050.

[22] H.K. Jang, J. Kim, J.S. Park, J.B. Moon, J. Oh, W.K. Lee, M.G. Kang, Synthesis and characterization of a conductive polymer blend based on PEDOT:PSS and its electromagnetic applications, Polymers 14 (2022), https://doi.org/10.3390/polym14030393.

[23] L. Liu, L. Wu, H. Yang, H. Ge, J. Xie, K. Cao, G. Cheng, S. Chen, Conductivity and stability enhancement of PEDOT:PSS electrodes via facile doping of sodium 3-methylsalicylate for highly efficient flexible organic light-emitting diodes, ACS Appl. Mater. Interfaces 14 (2022) 1615–1625, https://doi.org/10.1021/acsami.1c21591.

[24] A. Moazzeni, S. hamedi, Z. Kordrostami, Switching characteristic of fabricated nonvolatile bipolar resistive switching memory (ReRAM) using PEDOT: PSS/go, Solid State Electron. 188 (2022), https://doi.org/10.1016/j.sse.2021.108208.

[25] J.A. Ávila-Niño, E. Segura-Cárdenas, A.O. Sustaita, I. Cruz-Cruz, R. López-Sandoval, M. Reyes-Reyes, Nonvolatile write-once-read-many-times memory device with functionalized-nanoshells/PEDOT:PSS nanocomposites, Mater. Sci. Eng. B 176 (2011) 462–466, https://doi.org/10.1016/j.mseb.2011.01.006.

[26] C. Duan, Z. Liu, L. Yuan, H. Zhu, H. Luo, K. Yan, PEDOT:PSS-Metal oxide composite electrode with regulated wettability and work function for high-performance inverted perovskite solar cells, Adv. Opt. Mater. 8 (2020) 2000216, https://doi.org/10.1002/adom.202000216.

[27] W. Lee, S. Lee, H. Kim, Y. Kim, Organic thermoelectric devices with PEDOT:PSS/ZnO hybrid composites, Chem. Eng. J. 415 (2021) 128935, https://doi.org/10.1016/j.cej.2021.128935.

[28] A.V. Kukhta, A.E. Pochtenny, A.V. Misevich, I.N. Kukhta, E.M. Semenova, S.A. Vorobyova, E. Sarantopoulou, Optical and electrophysical properties of nanocomposites based on PEDOT: PSS and gold/silver nanoparticles, Phys. Solid State 56 (2014) 827–834, https://doi.org/10.1134/S1063783414040131.

[29] Y. Yang, H. Deng, Q. Fu, Recent progress on PEDOT:PSS based polymer blends and composites for flexible electronics and thermoelectric devices, Mater. Chem. Front. 4 (2020) 3130–3152, https://doi.org/10.1039/d0qm00308e.

[30] G. Biddeci, G. Spinelli, P. Colomba, F. Di Blasi, Nanomaterials: a review about halloysite nanotubes, properties, and application in the biological field, Int. J. Mol. Sci. 23 (2022), https://doi.org/10.3390/ijms231911518.

[31] J. Huang, Z.H. Tang, X.H. Zhang, B.C. Guo, Halloysite polymer nanocomposites, in: Dev. Clay Sci., Elsevier, 2016, pp. 509–553.

[32] M.S. Saharudin, S. Hasbi, M.N.A. Nazri, F. Inam, A review of recent developments in mechanical properties of polymer–clay nanocomposites, in: Lect. Notes Mech. Eng., 2020, https://doi.org/10.1007/978-981-15-5753-8_11.

[33] D. Tan, P. Yuan, D. Liu, P. Du, Surface modifications of halloysite, Dev. Clay Sci. 7 (2016) 167–201, https://doi.org/10.1016/B978-0-08-100293-3.00008-X.

[34] P. Yuan, D. Tan, F. Annabi-Bergaya, Properties and applications of halloysite nanotubes: recent research advances and future prospects, Appl. Clay Sci. 112–113 (2015) 75–98, https://doi.org/10.1016/j.clay.2015.05.001.

[35] M.J. Saif, H.M. Asif, M. Naveed, Properties and modification methods of halloysite nanotubes: a state-of-The-art review, J. Chil. Chem. Soc. 63 (2018) 4109–4125, https://doi.org/10.4067/s0717-97072018000304109.

[36] A.C. Santos, C. Ferreira, F. Veiga, A.J. Ribeiro, A. Panchal, Y. Lvov, A. Agarwal, Halloysite clay nanotubes for life sciences applications: from drug encapsulation to bioscaffold, Adv. Colloid Interface Sci. 257 (2018), https://doi.org/10.1016/j.cis.2018.05.007.

[37] E. Abdullayev, Y. Lvov, Halloysite for controllable loading and release, Dev. Clay Sci. 7 (2016) 554–605, https://doi.org/10.1016/B978-0-08-100293-3.00022-4.

[38] A.N. Reshetilov, A.E. Kitova, S.E. Tarasov, Y.V. Plekhanova, A.G. Bykov, A.K. Sundramoorthy, I.E. Kuznetsova, V.V. Kolesov, P.M. Gotovtsev, Highly conductive polymer PEDOT:PSS - application in biomedical and bioelectrochemical systems, Energy Environ. Sci. 12 (2020) 471–482, https://doi.org/10.17725/RENSIT.2020.12.471.

[39] M. Chozhanathmisra, D. Govindaraj, P. Karthikeyan, K. Pandian, L. Mitu, R. Rajavel, Fabrication of bilayer coating of poly(3,4-ethylenedioxythiophene)-halloysite/chitosan and Mg^{2+}/Sr^{2+} -doped HAP on titanium alloy for biomedical implant applications: physicochemical and *in vitro* biological performances studies, J. Chem. 2018 (2018) 1–12, https://doi.org/10.1155/2018/9813827.

[40] F. Hu, H. Peng, S. Zhang, Y. Gu, B. Yan, S. Chen, PEDOT nanoparticles fully covered on natural tubular clay for hierarchically porous electrochromic film, Sol. Energy Mater. Sol. Cells 199 (2019) 59–65, https://doi.org/10.1016/j.solmat.2019.04.017.

[41] A. Rosas-Aburto, I.A. Gabaldón-Saucedo, F. Espinosa-Magaña, M.T. Ochoa-Lara, P. Roquero-Tejeda, M. Hernández-Luna, J. Revilla-Vázquez, Intercalation of poly(3,4-ethylenedioxythiophene) within halloysite nanotubes: synthesis of composites with improved thermal and electrical properties, Microporous Mesoporous Mater. 218 (2015) 118–129, https://doi.org/10.1016/j.micromeso.2015.06.032.

[42] F. Wang, X. Zhang, Y. Ma, W. Yang, Synthesis of HNTs@PEDOT composites via in situ chemical oxidative polymerization and their application in electrode materials, Appl. Surf. Sci. 427 (2018) 1038–1045, https://doi.org/10.1016/j.apsusc.2017.08.155.

[43] F. Wang, X. Zhang, Y. Ma, D. Chen, W. Yang, Conductive HNTs-PEDOT hybrid preparation and its application in enhancing the dielectric permittivity of HNTs-PEDOT/PVDF composites, Appl. Surf. Sci. 458 (2018) 924–930, https://doi.org/10.1016/j.apsusc.2018.07.077.

[44] S.J. Luo, P. Zhang, Y.A. Mei, J.B. Chang, H. Yan, Electromagnetic interference shielding properties of PEDOT/PSS–halloysite nanotube (HNTs) hybrid films, J. Appl. Polym. Sci. 133 (2016), https://doi.org/10.1002/app.44242.

[45] P. Gemeiner, J. Kuliček, T. Syrový, A. Ház, V. Khunová, M. Hatala, M. Mikula, M. Hvojnik, L. Gál, M. Jablonský, M. Omastová, Screen-printed PEDOT:PSS/halloysite counter electrodes for dye-sensitized solar cells, Synth. Met. 256 (2019), https://doi.org/10.1016/j.synthmet.2019.116148.

[46] S. Tu, T. Tian, A. Lena Oechsle, S. Yin, X. Jiang, W. Cao, N. Li, M.A. Scheel, L.K. Reb, S. Hou, A.S. Bandarenka, M. Schwartzkopf, S.V. Roth, P. Müller-Buschbaum, Improvement of the thermoelectric properties of PEDOT:PSS films via DMSO addition and DMSO/salt post-treatment resolved from a fundamental view, Chem. Eng. J. 429 (2022) 132295, https://doi.org/10.1016/j.cej.2021.132295.

[47] S.-J. Luo, P. Zhang, Y.-A. Mei, J.-B. Chang, S. Ichikawa, K. Oshima, N. Toshima, H. Yan, Thermoelectric properties of PEDOT/PSS-halloysite nanotubes (HNTs) hybrid films, Curr. Nanosci. 13 (2017), https://doi.org/10.2174/1573413712666161025123550.

[48] H. Yan, P. Zhang, J. Li, X.L. Zhao, K. Zhang, B. Zhang, PEDOT/PSS-Halloysite nanotubes (HNTs) hybrid films: insulating HNTs enhance conductivity of the PEDOT/PSS films, Sci. Rep. 5 (2015), https://doi.org/10.1038/srep18641.
[49] C. Yegin, W. Lu, B. Kheireddin, M. Zhang, P. Li, Y. Min, H.-J. Sue, M. Murat Sari, M. Akbulut, The effect of nanoparticle functionalization on lubrication performance of nanofluids dispersing silica nanoparticles in an ionic liquid, J. Tribol. 139 (2017) 041802, https://doi.org/10.1115/1.4035342.
[50] A.B. Gurav, Q. Xu, S.S. Latthe, R.S. Vhatkar, S. Liu, H. Yoon, S.S. Yoon, Superhydrophobic coatings prepared from methyl-modified silica particles using simple dip-coating method, Ceram. Int. 41 (2015) 3017–3023, https://doi.org/10.1016/j.ceramint.2014.10.137.
[51] L.A. Beneditt-Jimenez, N.A. Ulloa-Castillo, J. Iturbe-Ek, O. Martínez-Romero, A. Elías-Zúñiga, A.O. Sustaita, A hybrid superhydrophobic/hydrophilic surface based on SiO2 nanoparticles over a clay substrate for enhanced dew yield potential, Appl. Sci. 12 (2022) 1526, https://doi.org/10.3390/app12031526.
[52] Z. Zhou, L. Fang, Y. Cao, W. Wang, J. Wang, Y. Yang, Y. Liu, Determination of Hansen solubility parameters of halloysite nanotubes and prediction of its compatibility with polyethylene oxide, Colloids Surf. A Physicochem. Eng. Asp. 601 (2020) 125031, https://doi.org/10.1016/j.colsurfa.2020.125031.
[53] Y. Mochizuki, T. Horii, H. Okuzaki, Effect of pH on structure and conductivity of PEDOT/PSS, Trans. Mater. Res. Soc. Jpn. 37 (2012) 307–310, https://doi.org/10.14723/tmrsj.37.307.
[54] Y. Lvov, E. Abdullayev, Functional polymer–clay nanotube composites with sustained release of chemical agents, Prog. Polym. Sci. 38 (2013) 1690–1719, https://doi.org/10.1016/j.progpolymsci.2013.05.009.
[55] S. Sarkar, A.C. Bhowal, R. Kandimalla, S. Kundu, Structural and electrical behaviours of PEDOT:PSS thin films in presence of negatively charged gold and silver nanoparticles: a green synthesis approach, Synth. Met. 279 (2021) 116848, https://doi.org/10.1016/j.synthmet.2021.116848.
[56] M. Pollak, B.I. Shklovskii, Hopping Transport in Solids, 1991.
[57] B.E. Kilbride, J.N. Coleman, J. Fraysse, P. Fournet, M. Cadek, A. Drury, S. Hutzler, S. Roth, W.J. Blau, Experimental observation of scaling laws for alternating current and direct current conductivity in polymer-carbon nanotube composite thin films, J. Appl. Phys. 92 (2002) 4024–4030, https://doi.org/10.1063/1.1506397.
[58] J. Hwang, D.B. Tanner, I. Schwendeman, J.R. Reynolds, Optical properties of nondegenerate ground-state polymers: three dioxythiophene-based conjugated polymers, Phys. Rev. B - Condens. Matter Mater. Phys. 67 (2003) 115205, https://doi.org/10.1103/PhysRevB.67.115205.
[59] L. Zekri, N. Zekri, R. Bouamrane, F. Brouers, Statistical and scaling properties of the alternating-current conductivity in thin metal-dielectric composites, J. Phys. Condens. Matter 12 (2000) 293–301, https://doi.org/10.1088/0953-8984/12/3/308.
[60] N. Pirouzfam, K. Sendur, Tungsten based spectrally selective absorbers with anisotropic rough surface texture, Nanomaterials 11 (2021) 2018, https://doi.org/10.3390/nano11082018.
[61] P. Sakunpongpitiporn, K. Phasuksom, N. Paradee, A. Sirivat, Facile synthesis of highly conductive PEDOT:PSS: via surfactant templates, RSC Adv. 9 (2019) 6363–6378, https://doi.org/10.1039/c8ra08801b.
[62] Q. Zhao, R. Jamal, L. Zhang, M. Wang, T. Abdiryim, The structure and properties of PEDOT synthesized by template-free solution method, Nanoscale Res. Lett. 9 (2014), https://doi.org/10.1186/1556-276X-9-557.
[63] Y. Liu, Y. Tang, P. Wang, H. Zeng, Carbonaceous halloysite nanotubes for the stabilization of Co, Ni, Cu and Zn in river sediments, Environ. Sci.: Nano 6 (2019) 2420–2428, https://doi.org/10.1039/c9en00326f.
[64] B. Szczepanik, P. Słomkiewicz, M. Garnuszek, K. Czech, D. Banas, A. Kubala-Kukus, I. Stabrawa, The effect of chemical modification on the physico-chemical characteristics of halloysite: FTIR, XRF, and XRD studies, J. Mol. Struct. 1084 (2015) 16–22, https://doi.org/10.1016/j.molstruc.2014.12.008.
[65] R.L. Frost, J. Kristof, J.M. Schmidt, J.T. Kloprogge, Raman spectroscopy of potassium acetate-intercalated kaolinites at liquid nitrogen temperature, Spectrochim. Acta Part Mol. Biomol. Spectrosc. 57 (2001) 603–609, https://doi.org/10.1016/S1386-1425(00)00382-6.
[66] M.T. Connor, S. Roy, T.A. Ezquerra, F.J. Baltá Calleja, Broadband ac conductivity of conductor-polymer composites, Phys. Rev. B 57 (1998) 2286–2294, https://doi.org/10.1103/PhysRevB.57.2286.
[67] J.C. Dyre, The random free-energy barrier model for ac conduction in disordered solids, J. Appl. Phys. 64 (1988) 2456–2468, https://doi.org/10.1063/1.341681.
[68] R.B. Laibowitz, Y. Gefen, Dynamic scaling near the percolation threshold in thin Au films, Phys. Rev. Lett. 53 (1984) 380–383, https://doi.org/10.1103/PhysRevLett.53.380.
[69] E. Abdullayev, Y. Lvov, Halloysite clay nanotubes for controlled release of protective agents, J. Nanosci. Nanotechnol. 11 (2011) 10007–10026, https://doi.org/10.1166/jnn.2011.5724.
[70] V. Bertolino, G. Cavallaro, G. Lazzara, M. Merli, S. Milioto, F. Parisi, L. Sciascia, Effect of the biopolymer charge and the nanoclay morphology on nanocomposite materials, Ind. Eng. Chem. Res. 55 (2016) 7373–7380, https://doi.org/10.1021/acs.iecr.6b01816.
[71] D. Antiohos, G. Folkes, P. Sherrell, S. Ashraf, G.G. Wallace, P. Aitchison, A.T. Harris, J. Chen, A.I. Minett, Compositional effects of PEDOT-PSS/single walled carbon nanotube films on supercapacitor device performance, J. Mater. Chem. 21 (2011) 15987, https://doi.org/10.1039/c1jm12986d.
[72] S.N. Karri, P. Srinivasan, Synthesis of PEDOT:PSS using benzoyl peroxide as an alternative oxidizing agent for ESD coating and electro-active material in supercapacitor, Mater. Sci. Energy Technol. 2 (2019) 208–215, https://doi.org/10.1016/j.mset.2019.01.008.
[73] J.L. Carter, C.A. Kelly, M.J. Jenkins, Processing optimization of PEDOT:PSS and PEDOT:PSS/Tween 80 films, Polym. J. 55 (2023) 253–260, https://doi.org/10.1038/s41428-022-00740-x.
[74] C.J. Lee, I.S. Tsai, Preparation and properties of PEDOT/PSS conductive polymer blended with graphene/PVDF, Adv. Mater. Res. 608–609 (2012) 1318–1326, https://doi.org/10.4028/www.scientific.net/AMR.608-609.1318.
[75] Y. Fan, T. Wang, R. Asrosa, B. Li, N. Naresh, X. Liu, S. Guan, R. Li, M. Wang, I.P. Parkin, B.D. Boruah, Synergistic contribution of activated carbon and PEDOT:PSS in hybrid electrodes for high-performance planar micro-supercapacitors, Chem. Eng. J. 488 (2024) 150672, https://doi.org/10.1016/j.cej.2024.150672.
[76] I. Ivanko, J. Pánek, J. Svoboda, A. Zhigunov, E. Tomšík, Tuning the photoluminescence and anisotropic structure of PEDOT, J. Mater. Chem. C 7 (2019) 7013–7019, https://doi.org/10.1039/C9TC00955H.
[77] B. Friedel, P.E. Keivanidis, T.J.K. Brenner, A. Abrusci, C.R. McNeill, R.H. Friend, N.C. Greenham, Effects of layer thickness and annealing of PEDOT:PSS layers in organic photodetectors, Macromolecules 42 (2009) 6741–6747, https://doi.org/10.1021/ma901182u.
[78] H.S. Kang, S.-Y. Park, K. Kim, J.-W. Kim, H. Jeong, S.H. Lee, M.-H. Lee, Preparation of PEDOT/PSSA conductive nanoparticles for dielectrophoretic display, Macromol. Res. 21 (2013) 693–698, https://doi.org/10.1007/s13233-013-1060-3.
[79] X. Lyu, B. Clark, A.M. Peterson, Thermal transitions in and structures of dried polyelectrolytes and polyelectrolyte complexes, J. Polym. Sci., Part B: Polym. Phys. 55 (2017) 684–691, https://doi.org/10.1002/polb.24319.
[80] A. Anand, J.P. Madalaimuthu, M. Schaal, F. Otto, M. Gruenewald, S. Alam, T. Fritz, U.S. Schubert, H. Hoppe, Why organic electronic devices comprising PEDOT:PSS electrodes should be fabricated on metal free substrates, ACS Appl. Electron. Mater. 3 (2021) 929–943, https://doi.org/10.1021/acsaelm.0c01043.